Atmospheric Research 238 (2020) 104870

Contents lists available at ScienceDirect

Atmospheric Research

journal homepage: www.elsevier.com/locate/atmosres

The effect of considering polar vortex dynamics in the validation of satellite total ozone observations

Peristera Paschou[a,*], Maria-Elissavet Koukouli[a], Dimitrios Balis[a], Christophe Lerot[b], Michel Van Roozendael[b]

[a] Laboratory of Atmospheric Physics, Aristotle University of Thessaloniki, 54124 Thessaloniki, Greece
[b] Royal Belgian Institute for Space Aeronomy, 3, Avenue Circulaire, 1180 Brussels, Belgium

ARTICLE INFO

Keywords:
Total ozone column
GOME2
OMI
Validation
Potential vorticity

ABSTRACT

The main aim of this paper is to demonstrate the magnitude in which validation results of space-based total ozone column, TOC, measurements are affected by the location of the polar vortex. Potential Vorticity is used as an indicator to determine the polar vortex's boundary and surface area, provided by ERA-Interim reanalysis datasets from the European Centre for Medium-Range Weather Forecasts (ECMWF). The total ozone measurements that were examined fall within the hemispherical winter-spring period, focusing on middle and high latitudes on both hemispheres. The space-based total ozone data produced by the GODFIT (GOME-type Direct FITting) v4 algorithm as applied to the OMI/Aura, GOME-2/Metop-A and Metop-B observations, part of the European Space Agency's Ozone Climate Change Initiative project, are compared to TOC measurements from Brewer and Dobson spectrophotometers archived at the World Ozone and Ultraviolet Radiation Data Centre (WOUDC) repository. The satellite-to-ground collocations were classified depending on whether both satellite and ground-based measurements are inside or outside the polar vortex (matched) or one measurement is inside whereas the other one is outside the polar vortex (mismatched). It is shown that the matched cases present an improved agreement between satellite and ground TOC measurements compared to the mismatched cases. Considering all examined stations for GOME2-A, GOME2-B, and OMI, the mean bias for the mismatched cases was found to be 2.22 ± 0.4%, 1.84 ± 0.57%, and 1.93 ± 0.39% respectively, while for the matched cases was found to be 1.46 ± 0.17%, 1.69 ± 0.22%, 1.7 ± 0.19% respectively. For the three satellite sensors, the mismatched cases do not exceed 3.3% of the total available collocations per station during the winter-spring period between years 2007 and 2017, where applicable. Hence, on a global scale, the exclusion of mismatched collocated measurements does not cause significant changes and the resulting impact on the validation of the satellite TOCs is small. However, when considering single stations consistently affected by the polar vortex, we conclude that mismatched cases should be excluded from the comparisons.

1. Introduction

Despite its relatively small concentration, stratospheric ozone is a key element of the Earth's atmosphere since, as a strong absorber of solar ultraviolet (UV) radiation between 200 and 300 nm, it acts as a protective shield of the incoming UV radiation for the organic life on Earth (Hewitt and Jackson, 2009). Ozone forms a protective shield, known as the ozone layer, that reduces the intensity of solar UV radiation that reaches the Earth's surface, determines the vertical profile of temperature in the atmosphere and is directly involved in numerous stratospheric chemical reactions (Wallace and Hobbs, 2006).

According to the World Ozone and Ultraviolet Radiation Data Centre's (WOUDC) data archive (https://woudc.org/data/instruments/), systematic ground-based measurements of total ozone columns (TOC) began in the early 1920s by the Dobson spectrophotometers. In the early 1980s, Brewer spectrophotometers were further deployed and also began to monitor total ozone levels, while in the early 1990s the Système d'Analyse par Observations Zénithales (SAOZ, Pommereau and Goutail, 1988) started to provide routine observations in key locations. To add to the ground-based monitoring capabilities, since the 1970s, a number of space-borne UV monitoring instruments were placed in orbit, starting with the Backscatter UltraViolet (BUV) instrument on board the National Aeronautics and Space Administration's (NASA) satellite Nimbus-4 and followed by a continuous series of sensors until

* Corresponding author at: Institute of Astronomy, Astrophysics, Space Applications and Remote Sensing, National Observatory of Athens, 15236 Athens, Greece.
E-mail address: pepascho@physics.auth.gr (P. Paschou).

https://doi.org/10.1016/j.atmosres.2020.104870
Received 14 April 2019; Received in revised form 16 January 2020; Accepted 20 January 2020
Available online 22 January 2020
0169-8095/

NOAA 19 SBUV/2 in orbit and operational since 2009 (see for e.g. Bhartia et al., 2013). Similarly, the Total Ozone Mapping Spectrometer (TOMS) has flown consecutively on Nimbus-7 in 1979, Meteor-3 in 1994 and on Earth Probe on 1996. Launched in 2004 on board Aura, the Ozone Monitoring Instrument (OMI) is still active alongside the Suomi NPP OMPS launched in 2011. In Europe, the GOME-2 suite of instruments [on EUMETSAT (European Organisation for the Exploitation of Meteorological Satellites) MetopA in 2007, MetopB in 2013 and MetopC in 2018] continue to monitor the ozone layer as well as numerous other species in the UV/Vis part of the spectrum (see for e.g. Flynn et al., 2009; Hassinen et al., 2016; Levelt et al., 2018).

Extensive scientific studies but also routine validation efforts have been performed in the last two decades with the aim to assess the quality of the satellite total ozone data using collocated ground-based data. From these studies, issues within the individual datasets were identified which helped to improve the algorithms and revise the satellite datasets (see for e.g. Balis et al., 2007a, b; Garane et al., 2018; Koukouli et al., 2015; Loyola et al., 2011). Of direct interest to this work, Hansen et al. (1999), validated GOME/ERS-2 total ozone measurements in high latitude stations from the Norwegian ozone monitoring network and revealed deviations of the GOME total ozone data from ground-based data which depended on solar zenith angle and season. As a plausible explanation for the latter was the geophysical variability of the polar vortex and the insufficient capability of the GOME algorithm (version 2) used in the study to properly account for it. According to Hansen et al. (1999) the observed deviations during winter and spring time are related to abrupt changes in total ozone within a day -or a few days- caused by the position of the polar vortex and its rapid displacement attributed to subtropical intrusions (Baldwin and Holton, 1988; Hood et al., 1999; Schoeberl and Hartmann, 1991). The direct impact of this geophysical situation is that the total ozone content varies considerably. The indirect impact is that other atmospheric parameters such as temperature, air pressure and ozone vertical distribution, relevant for the total ozone algorithm via the air mass factor calculation, change significantly in the vortex edge region. These parameters were not properly represented by the climatology used in the GOME algorithm studied in Hansen et al. (1999), and may have contributed to the observed deviations in winter and spring. It hence follows that the precise position of polar vortex may affect validation results as the satellite and the ground-based station may see different air masses, one located inside the polar vortex whereas the other one located outside the polar vortex.

The polar vortex is a large-scale region of air that is contained by a strong westerly jet stream (polar night jet) that circles the polar region; as a winter phenomenon over the poles in the stratosphere, it is strongly associated with the ozone hole characteristics (Wallace and Hobbs, 2006). In the Southern Hemisphere, the polar vortex is formed during austral winter (June–September) whereas, typically, by late December it disappears. On the other hand, in the Northern Hemisphere the polar vortex is well formed until late November and breaks up by late April (Nash et al., 1996). A quantitative method for determining the polar vortex boundary and its width is defined by Nash et al. (1996) by using the distributions of Potential Vorticity, PV, on isentropic surfaces. Potential Vorticity is a conserved quantity on isentropic surfaces in absence of diabatic and frictional processes, derived from temperature and wind fields. The potential vorticity is either given per SI units ($K{\cdot}m^2{\cdot}kg^{-1}{\cdot}s^{-1}$) or the potential vorticity unit (PVU), where 1 PVU = $10^{-6}{\cdot}K{\cdot}m^2{\cdot}kg^{-1}{\cdot}s^{-1}$. The boundary between polar vortex and mid-latitude air is indicated by the position of the strong horizontal gradient of PV on an isentropic surface. Inside the polar vortex the PV values increasing poleward, while, outside of the polar vortex, in midlatitudes, the PV values and gradients are smaller.

The main aim of this paper is to demonstrate the magnitude in which modern, high spatial resolution, space-based TOC validation results are affected in the cases where the collocation criteria result in either set of the observations being affected by the location of the polar vortex.

2. Total ozone column observations and potential vorticity estimates

A brief description of the three datasets used in the study and the method applied is given in the subsections below.

2.1. Satellite TOC observations

The satellite data sets (level-2 total ozone data products) consist in retrievals from GOME2/Metop-A, GOME2/Metop-B and OMI/Aura observations by the European Space Agency (ESA) Ozone_CCI GODFIT (GOME-type direct fitting) v.4 algorithm (Lerot et al., 2010). These data products have already been validated on a global scale against ground-based instruments (Garane et al., 2018). The two Global Ozone Monitoring Instrument (GOME2) sensors, operating in tandem, are flying onboard EUMETSAT's MetOp-A and MetOp-B satellites while the Ozone Monitoring Instrument (OMI) is flying onboard NASA's Earth Observing System (EOS) Aura satellite. Further details on the missions, the GOME2 and OMI instruments, as well as their scientific findings, can be found in Hassinen et al. (2016) and Munro et al. (2016) for GOME2 and in Levelt et al. (2018) for OMI.

In Table 1, the characteristics of each satellite instrument considered in the direct comparisons are presented. Differences in the estimated total ozone can be a result of differences in the level-1 products, in the instruments and satellites themselves and therefore such differences should be taken into account when comparing two satellite datasets (Hassinen et al., 2016). The differential signal-to-noise characteristics of the instruments as well as the different degradation effects can also have an impact on the total ozone column retrieval (Hassinen et al., 2016).

The GODFIT v.4 algorithm is the baseline algorithm for total ozone retrieval from backscatter UV sensors, such as GOME-2 and OMI for the ESA Ozone_CCI project (http://www.esa-ozone-cci.org/). This project aims at generating high quality and fully traceable, long-term data records of ozone measurements from all relevant ESA, EUMETSAT and Third Party Missions. The GODFIT algorithm was jointly developed at BIRA-IASB (Royal Belgian Institute for Space Aeronomy), DLR-IMF (German Aerospace Center) and RT-Solutions for implementation in version 5 of the GOME Data Processor (GDP) operational system (Van Roozendael et al., 2012). In contrast to previous versions of the GDP, which were based on the Differential Optical Absorption Spectroscopy (DOAS) method, GODFIT uses a least-squares fitting inverse algorithm including direct multi-spectral radiative transfer simulation of earthshine radiances and Jacobians with respect to total ozone, albedo closure and other ancillary fitting parameters (Van Roozendael et al., 2012). Further details on the GODFIT algorithm can be found in Lerot et al. (2010, 2014). According to Garane et al. (2018) the individual

Table 1
Main characteristics of the GOME2/MetOp-A, GOME2/MetOp-B and OMI/Aura instruments.

	GOME-2/MetOp-A	GOME-2/MetOp-B	OMI/Aura
In orbit since	10/2006	9/2012	7/2004
Spectral resolution	0.26–0.51 nm	0.26–0.51 nm	0.42–0.63 nm
Spatial resolution (default)	80 × 40 km^2 40 × 40 km^2 since July 15, 2013	80 × 40 km^2	13 × 24 km^2
Swath width	1920 km 960 km since July 15, 2013	1920 km	2600 km
Equatorial crossing time	09:30 LT	09:30 LT	13:45 LT
Level-1-to-2 algorithm	GODFITv.4	GODFITv.4	GODFIT v.4

level-2 total ozone datasets show excellent intersensor consistency with mean differences within 1.0% at moderate latitudes (± 50°).The mean bias between GODFIT v.4 satellite and ground based TOCs is well within 1.5 ± 1.0% for all sensors, such as OMI/Aura, GOME-2/Metop-A and /Metop-B among others. Thus, the observed inter-sensor consistency renders the level-2 total ozone datasets retrieved by GODFIT v.4, suitable and useful for long-term analysis of the ozone layer.

2.2. Ground-based TOC observations

Archived global Brewer and Dobson total ozone column measurements from the WMO/Global Atmosphere Watch, GAW, network, routinely deposited at the WOUDC, https://woudc.org/, in Toronto, Canada, were used as ground reference in this study.

The Dobson instrument is a manually operated double monochromator with a dispersing spectrometer and a recombining spectrometer specifically designed for TOC measurements (Staehelin et al., 2003). The use of the double monochromator minimizes stray light scattered internally within the instrument. The most precise measurements of TOC can be obtained by direct sun observations, although TOCs can also be determined from blue or cloudy zenith sky measurements with lower precision. In contrast, the Brewer instruments are in principle similar to the Dobson instrument, with more modern technology and are fully automated, requiring less manual labour (Staehelin et al., 2003). An automated sun tracker within the Brewer instruments aligns the instrument into the proper position for each type of measurement. Brewers can also make measurements of other important atmospheric parameters such as sulfur dioxide (SO_2) (Kerr et al., 1981) and nitrogen dioxide (NO_2) (Cede et al., 2006; Diémoz et al., 2014). Many of stations with Dobson instruments have added Brewer instruments to their measurement program. As shown in Garane et al. (2018), for the Dobson network, all time series of TOC measurements present a rather consistent and stable behavior with a bias of 1.26 ± 0.81%, 1.20 ± 1.04% and 1.45 ± 1.08% for OMI, GOME-2A and GOME-2B respectively. For the Brewer network, the consistency and the stability of the satellite measurements is also evident for the whole time period of available data where the overall bias of the individual comparisons is 1.18 ± 0.50%, 1.08 ± 0.75% and 1.59 ± 0.69% for OMI, GOME-2A and GOME-2B respectively.

Measurements by both types of instruments are based on sun photometry and the TOC is derived from the absorption of solar light in the Huggins band. However, the Dobson spectrophotometer is based on the measurements of the ratios of two wavelength pairs (305.5/325.4 nm and 317.6/339.8 nm), while the Brewer spectrophotometer measures photocounts at 5 wavelengths (306.3 nm, 310.1 nm, 313.5 nm, 316.8 nm and 320.1 nm), allowing the simultaneous measurement of both ozone and SO_2 columnar amounts. The wavelengths used in the TOC measurements in Dobson spectrophotometry are more sensitive to stratospheric temperature variations than those of the Brewer instrument because of the different choice of wavelength combination used (Staehelin et al., 2003). Koukouli et al. (2016) discussed the dependency of the stratospheric effective temperature on TOC measurements from Dobson spectrometers, which manifests itself in the comparisons as a seasonality effect. The measurements originated from Dobson instruments were corrected with the appropriate effective temperature and the comparisons improved considerably, i.e. from the 0.63 ± 0.66% to the 0.26 ± 0.46% in the Northern Hemisphere and from 1.25 ± 1.20% to 0.80 ± 0.71% in the Southern Hemisphere (Koukouli et al., 2016). The calibration of the Brewer and Dobson instruments is based on the Langley plot calibration at the Mauna Loa Observatory at Hawaii, but the operating procedures differ for the two networks (Staehelin et al., 2003). Except of the Mauna Loa Observatory, there is also the Regional Brewer Calibration Center-Europe (RBCC-E) at the Izaña Atmospheric Observatory at Canary Islands, where many of Brewer instruments have been calibrated from RBCC-E during campaigns, e.g. in Huelva in 2014 (Redondas et al., 2018).

Measurements from the ground-based network of Dobson and Brewer instruments are commonly used as a reference for satellite comparisons. A continuously updated selection of these Brewer and Dobson measurements has already been used numerous times in the validation and analysis of global total ozone records (see for e.g. Balis et al., 2007a; Garane et al., 2018; Koukouli et al., 2015; Kramarova et al., 2013; Labow et al., 2013; Loyola et al., 2011).

2.3. Potential vorticity estimates

The PV data set is provided by ERA-Interim reanalysis datasets from the European Centre for Medium-Range Weather Forecasts (ECMWF), https://www.ecmwf.int/. ERA-Interim is a reanalysis of the global atmosphere covering the time period from 1979 until 2018. The ERA-Interim atmospheric model and reanalysis system uses the ECMWF's Integrated Forecast System (IFS) version cy31r2, which was introduced operationally in September 2006. The spatial resolution of the data is 60 vertical levels from the surface up to 0.1 hPa, with spherical-harmonic representation for the basic dynamical fields and a reduced Gaussian grid with approximately uniform 79 km spacing for surface and other grid-point fields (Berrisford et al., 2011). The data assimilation system includes a 4-dimensional variational analysis (4D-Var) with a 12-hour analysis window, which outputs at 4 time stamps at 00:00, 06:00, 12:00 and 18:00 UTC.[1] In this study, daily advected PV fields (0.25° × 0.25°) at the 475 K potential temperature surface are used to define the position of the polar vortex, the edge and its surface area. This isentropic level, which corresponds to approximately 16.4 km altitude, represents a mean level of the low stratosphere where the maximum ozone number density is observed (Parrondo et al., 2014) and was also used in previous studies (Bojkov et al., 1998; Parrondo et al., 2014). As shown in Fig. 1, in the Southern Hemisphere during hemispherical winter, the polar vortex is fully formed (yellow-red colors in the left panel) with the potential vorticity map on the 475 K surface of potential temperature and the ozone hole being notable (blue colors signify < 200 D.U.) covering almost the same area that polar vortex covers. Moreover, a slight displacement of the polar vortex towards the Atlantic Ocean is notable. A variability or a displacement in the polar vortex can be caused by large weather systems and/or Rossby waves, which are forced by the large-scale mountain systems and the land-sea contrasts between continents and oceans resulting in erosion of the polar vortex (Baldwin and Holton, 1988). Such displacement of the vortex away from the pole can affect regions in lower latitudes by transporting towards them, air masses from the vortex with significantly low ozone concentrations.

2.4. Methodology

In order to study the effect of the potential vorticity in the validation of satellite total ozone measurements by taking into account the formation and dissipation periods of the polar vortex in the two Hemispheres, the total ozone measurements that were examined fall within the hemispherical winter-spring period, e.g. from 1st November to 30th April for the Northern and from 1st April to 30th December for the Southern Hemisphere. The Southern winter-spring period is more expanded due to the fact that the Southern polar vortex is stronger, more persistent and nearly symmetric compared to the Northern polar vortex (Baldwin and Holton, 1988; Hood et al., 1999; Schoeberl and Hartmann, 1991).

Ozone observations from 2007 to 2017 were studied for Brewer and Dobson stations in the Northern and Southern Hemisphere. The stations were selected in accordance with the criteria discussed in detail in Balis et al. (2007a,b), focusing on latitudes greater than 30° or lower than −30°. Middle-latitude stations are included, since in cases of displacement of the polar vortex due to the propagation of planetary-scale waves

[1] https://www.ecmwf.int/en/forecasts/datasets/archive-datasets/reanalysis-datasets/era-interim

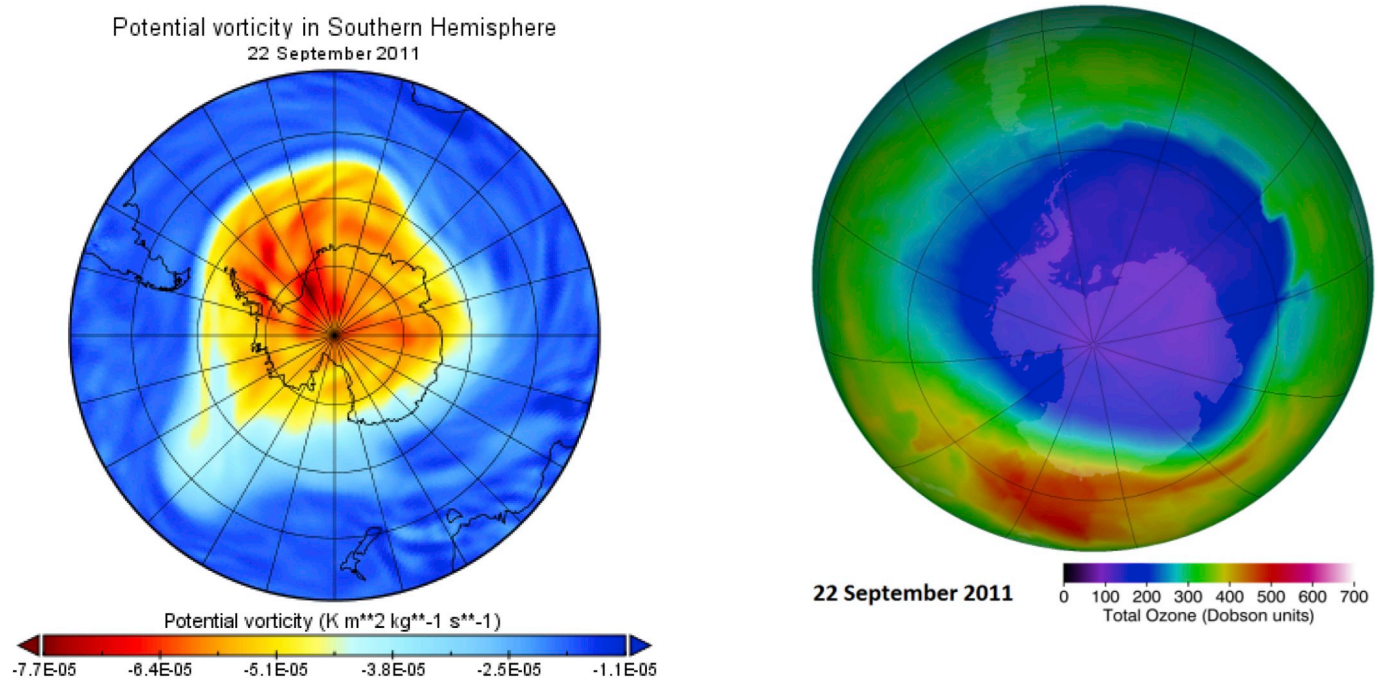

Fig. 1. Maps of potential vorticity (left panel) and total ozone (right panel) in Southern Hemisphere for the 22nd of September 2011. When the polar vortex is fully formed (yellow-red colors) in the left panel with the potential vorticity map on the 475 K surface of potential temperature, the ozone hole is notable (blue colors signify < 220 D.U.) as observed by OMI instrument onboard the Aura satellite (data gaps filled in with assimilated fields). [Ozone map adapted from https://ozonewatch.gsfc.nasa.gov/monthly/SH.html]. (For interpretation of the references to colour in this figure legend, the reader is referred to the web version of this article.)

or large weather systems, ozone at midlatitudes varies significantly both temporally and spatially (Hood et al., 1999; Schoeberl and Hartmann, 1991). All satellite pixels with their center coordinates laying within three discrete radii from each of the ground-based stations have been selected for the validation. The spatial criteria which were applied on the radius between the center satellite pixel, i.e. pixel's coordinates, and the ground-based station's coordinates depend on each sensor's spatial coverage. For GOME-2/Metop-A and GOME-2/Metop-B, since they have approximately the same ground pixel resolution, the radii of collocation were chosen as 50 km, 100 km and 150 km. For OMI/Aura, which is characterized by a higher spatial resolution, the radii of search were defined to be 12.5 km, 25 km and 50 km. Since the WOUDC data are provided on a daily mean basis, all satellite pixels spatially collocated with a station, were used to the comparison with the ground-based observations of the day.

The collocations between ground and satellite based measurement were separated depending on whether both satellite and ground-based measurements are inside or outside the polar vortex (hereafter, *matched*) or one measurement is inside whereas the other one is outside the polar vortex (hereafter, *mismatched*). The PV level was used as an indicator in this classification. For each pair of collocations between ground and satellite, the two measurements were matched with the corresponding PV value of the closest grid cell from the PV field with respect to the station's coordinates for the ground-based measurement and with respect to the pixel's coordinates for the satellite measurement. In order to determine if a measurement is inside or outside the polar vortex, the matched PV value with the measurement was compared with a critical PV value that defines the vortex boundary, namely the 42 PVU (Bojkov et al., 1998). If the absolute value of PV of the measurement is bigger than the PV critical value, then the measurement is considered to be inside the polar vortex, otherwise the measurement is assumed to be outside the polar vortex. In the Northern Hemisphere the critical value is 42 PVU, while, in the Southern Hemisphere is −42 PVU due to positive and negative PV values in the respective hemispheres (Berrisford et al., 2011).

After classification of each pair of collocations the percentage difference (bias) was calculated with respect to the ground-based measurement, i.e. the difference between satellite TOC measurement and ground-based TOC measurement divided by the ground-based TOC measurement, and statistical analyses were carried out for both matched and mismatched cases in order to investigate the effect of potential vorticity in validation. Stations with no mismatched collocation cases were excluded from the statistical analyses.

3. Results

The stations that were selected and used in the analysis, in accordance to the latitudinal selection and the criteria discussed in Balis et al. (2007a, 2007b), are 110 from 285 available stations provided by WOUDC's archive, consisting of 59 Brewer and 51 Dobson instruments. Details on these locations can be found in the Appendix. As shown in Fig. 2, the Brewer instruments [black dots] are almost all located in the Northern Hemisphere, except of a few, covering regions with maximum latitude of ~80°. The Dobson instruments [red squares] are more evenly distributed in the two hemispheres, however a large part of the number of stations is found approximately in the range between 30° and 70° in the Northern Hemisphere.

The number of stations that were found to provide matched and mismatched collocations in at least one of the three applied spatial criteria is 63 for GOME2-A, 44 for GOME2-B and 55 for OMI out of the total 110 stations that were examined.

3.1. Individual station analysis

Four stations per satellite sensor were selected as example for presenting the results of this work: one station in midlatitudes and one in high latitudes, for each Hemisphere. For the GOME2 sensors, the selected stations are Edmonton and Resolute in Canada, Comodoro Rivadavia in Argentina and Marambio in Antarctica. For the OMI sensor the selected stations are Goose in Canada, Vindeln in Sweden, Macquarie Island in Australia and Marambio in Antarctica. Different stations for the two types of satellite sensors were selected because for these stations, mismatched cases were found in all applied spatial criteria. In Table 2, the number of days, as well as the percentage of the

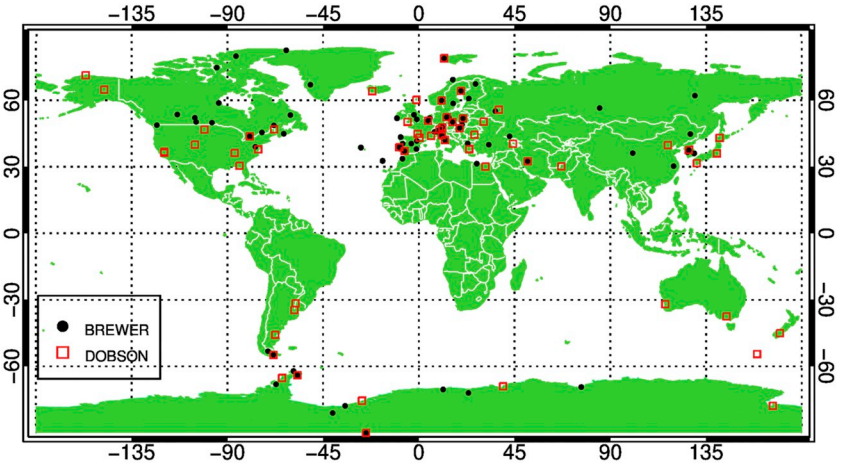

Fig. 2. Brewer [black dots] and Dobson [red squares] spectrophotometers providing both matched and mismatched collocations depending on the location of the polar vortex for either of the three satellite sensors. (For interpretation of the references to colour in this figure legend, the reader is referred to the web version of this article.)

Table 2
Number of days that the polar vortex covers [inside] or not [outside] the stations during the period 2007–2017.

Station	Latitude (°)	Inside polar vortex (days)	Time inside (%)	Outside polar vortex (days)	Time outside (%)
Comodoro Rivadavia	−45.75	11	0.3	4007	99.7
Goose	53.25	54	1.3	3964	98.7
Marambio	−64.00	1243	30.9	2775	69.1
Vindeln	64.25	271	6.7	3747	93.3

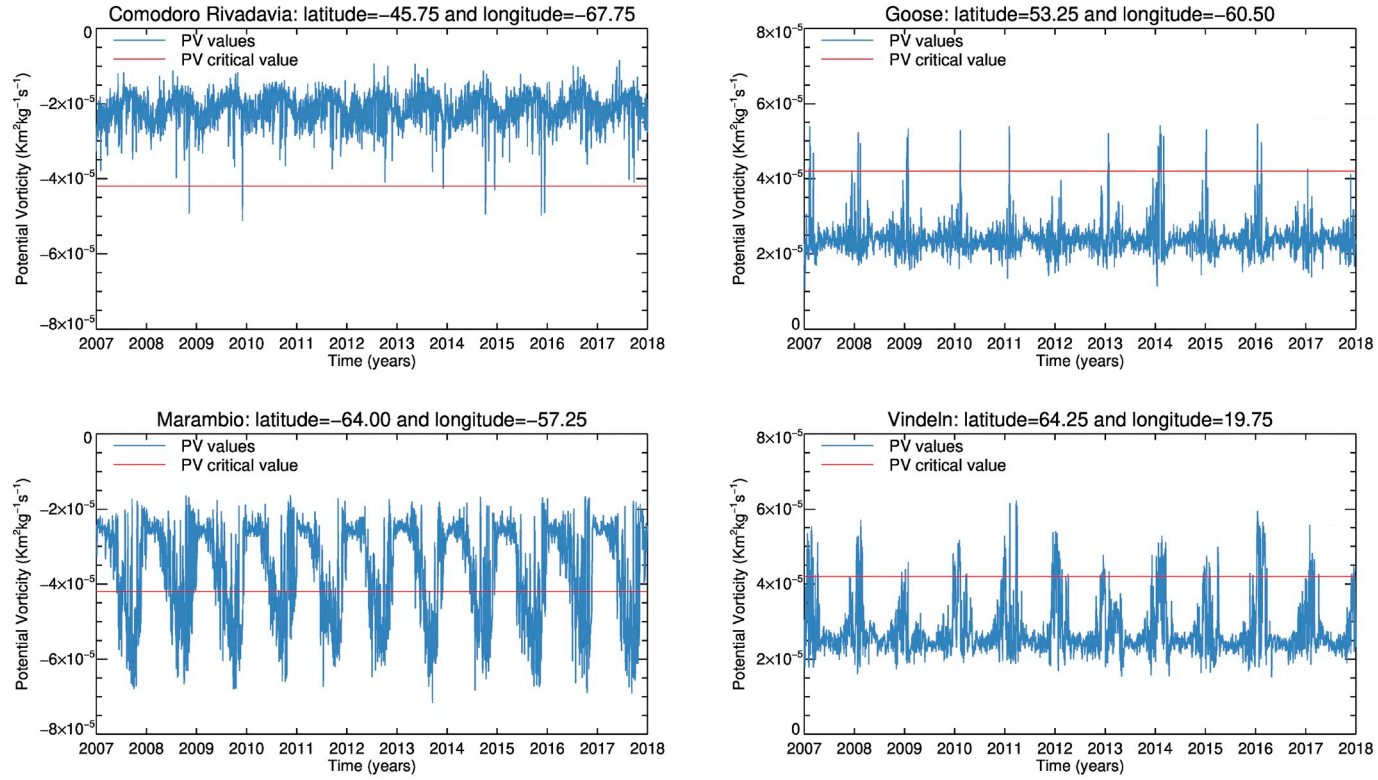

Fig. 3. Potential Vorticity (blue) as a function of time in two stations in middle latitudes, Comodoro Rivadavia (upper left) in Southern Hemisphere and Goose (upper right) in Northern Hemisphere and in two stations in high latitudes, Marambio (lower left) in Southern Hemisphere and Vindeln (lower right) in Northern Hemisphere. The PV critical value (red) in Southern Hemisphere is $-4.2{\cdot}10^{-5}$ km^2kg^{-1} s^{-1} and in Northern Hemisphere is $4.2{\cdot}10^{-5}$ km^2kg^{-1} s^{-1}. (For interpretation of the references to colour in this figure legend, the reader is referred to the web version of this article.)

2007–2017 period, the stations were inside and outside the polar vortex is shown. In Fig. 3 the potential vorticity time series over selected stations for the two Hemispheres is shown.

In Comodoro Rivadavia (Fig. 3 upper left) and Goose (Fig. 3 upper right), both located in the midlatitudes of the SH and the NH respectively, the PV values (in blue) do not exceed the critical value (red line) for most of the period between 2007 and 2017. In 4007 and 3964 out of 4018 days of the period 2007–2017 respectively the station is not covered by the polar vortex (Table 2). The few days, i.e. 11 in Comodoro Rivadavia and 54 in Goose, when the polar vortex covers the

stations, are located during hemispherical winter or early spring and are attributed to the displacement of the polar vortex due to propagation of planetary-scale waves (Baldwin et al., 1988). The difference in the number of days affected by the polar vortex in the two middle latitude stations (Table 2) is explained by the fact that the Goose station is closer to the polar region and in higher latitude than the Comodoro Rivadavia. In contrast, Marambio (Fig. 3 lower left) and Vindeln (Fig. 3 lower right), which are located at high latitudes of the SH and the NH respectively, are stations where the PV values (in blue) exceed the critical value (red line) every year during early spring or winter and the polar vortex covers the station for 1243 days for Marambio and 271 for Vindeln. From the latter, the formation of the polar vortex during winter and early spring over high latitude regions is confirmed. Furthermore the stronger persistence of the southern polar vortex compared to the northern polar vortex is evident, as Marambio is covered by the vortex 30.9% of the time while Vindeln in only covered by the vortex 6.7% of the examined period.

3.2. Mean Bias and statistical analysis

A quick view on how the potential vorticity levels can affect the validation of TOC measurements during winter-spring period, retrieved from OMI (left column) and GOME2-A (right column), is demonstrated in Fig. 4. The same analysis was also performed for the GOME2-B retrievals [not shown here]. In Fig. 4, the panels are as many as the spatial criteria that were applied per satellite sensor, in the radius between centered satellite pixel and the ground-based station's coordinates, i.e. radii < 12.5 km (top left panel), 25 km (middle left panel) and 50 km (bottom left panel) for OMI and < 50 km (top right panel), 100 km (middle right panel) and 150 km (bottom right panel) for GOME2-A. Each one of the figures shows the mean bias for the mismatched (open circle in red) and matched (filled diamond in blue) collocated measurements between ground and satellite for the Brewer network [Dobson not shown.] The weighted standard deviation as a function of latitude is shown only for the mismatched cases for clarity purposes.

Fig. 4 shows that the mean bias for the mismatched cases [red circles] is larger than the mean bias for the matched cases [blue diamonds] in absolute units in most of the stations for all applied spatial criteria for both GOME2-A [right column] and OMI [left column] retrievals. The larger differences between the mean bias for the mismatched and the matched are seen for the middle to high latitudes where the potential vorticity varies the most due to displacement of polar vortex and movement of its edge. This may be a first clue of how the polar vortex dynamics, considering the potential vorticity as an indicator of the location of the air masses seen by the satellite and the ground station with respect to the polar vortex, affect the validation results of satellite borne TOC measurements, as the exclusion of mismatched collocated measurements can lead to improved comparisons.

Since the statistics for the largest applied spatial collocation criterion, i.e. 150 km for GOME2 and 50 km for OMI is shown not to introduce artefacts and spurious points in the analysis, in order to increase our statistical sample, it is chosen henceforth for presenting the statistical analyses, figures and tables. In Tables 3, 4, and 5, the mean bias and the number (N) of matched and mismatched collocations during the winter-spring period are shown for GOME2-A, GOME2-B and OMI respectively. The distribution of the biases for each station as well as the potential drift of the distribution between matched and mismatched cases are presented in Fig. 5 for both GOME2 sensors and in Fig. 6 for OMI.

In all examined stations for GOME2-A, GOME2-B and OMI, the mean bias for the mismatched cases was averaged to 2.22 ± 0.4%, 1.84 ± 0.57% and 1.93 ± 0.39% respectively, while for the matched cases was averaged to 1.46 ± 0.17%, 1.69 ± 0.22%, 1.7 ± 0.19%, indicating a slightly better agreement between satellite and ground TOC measurements for the matched collocations than for the mismatched.

The difference in the bias between matched and mismatched cases per station is also depicted in Figs. 5 and 6, where the bias of the matched cases appears to follow a normal Gaussian distribution, while the distribution of the bias for the mismatched cases seems to be shifted in comparison to the matched cases, see e.g. the Edmonton case (middle panels in Fig. 5), or to be distorted as in Macquarie Island (left panel in Fig. 6) and Resolute (left panels in Fig. 5).

It should be noted however that the statistics in Tables 3, 4 and 5 have to be carefully considered: the number of mismatched cases in these four stations, as well as in all the examined stations, does not exceed 3.3%, 2.8% and 2.3% of the total available collocations during the winter-spring period for GOME2-A, GOME2-B and OMI respectively. Hence, the low percentage of mismatched cases in regard to the number of total collocations may not introduce remarkable differences if the global and even semi-hemispherical averages are studied. It is also to ensure sufficient statistics that the temporal window for the North Pole was set to be eight months instead of being restricted to the ozone hole period (roughly between September and December). We note that e.g. at the location of Halley Bay (-75°S), and for the ten years of GOME2-A observations, we end up with 838 mismatched collocations instead of 2902 if we restrict ourselves to the ozone hole months. Hence, even though the differences might have been more pronounced for the cases of low ozone conditions, we opted for a larger dataset for this study.

3.3. Scatter plots

In the following (Fig. 7), scatter plots are presented that show the ground-based TOC measurements (x axis) and the GOME2 TOC measurements (y axis) for the mismatched (red) and matched (blue) cases at three different stations. A linear regression was applied for both sets of measurements (matched and mismatched) and the correlation coefficient, the slope, and the intercept were calculated for both cases.

As shown in Fig. 7, the correlation coefficient for the matched cases ranges from approximately 0.9 to 0.98, while for the mismatched cases ranges from 0.63 to 0.99. Considering all examined stations, the correlation coefficient for the matched cases was found to be 0.94 ± 0.01 for GOME2-A and 0.94 ± 0.01 for GOME2-B, while for the mismatched cases was found to be 0.89 ± 0.02 for GOME2-A and 0.84 ± 0.03 for GOME2-B. In addition, in Fig. 7, the slope, viewed as the ratio of change in satellite TOC measurements per change in the ground-based TOC measurements, is closer to one in most matched cases compared to the slope for the mismatched collocations. The slope for matched cases ranges from 0.91 to 1.01, while for the mismatched cases ranges from 0.45 to 0.98. Considering all examined stations, the slope for the matched cases was found to be 0.95 ± 0.01 for GOME2-A and 0.96 ± 0.01 for GOME2-B, while for the mismatched cases was found to be 0.92 ± 0.03 for GOME2-A and 0.94 ± 0.04 for GOME2-B.

An interesting discrepancy can be found when examining the intercept, which can be interpreted as a systematic additive discrepancy between satellite measurements and reference ground-based measurements. In Fig. 7, in all stations except for Edmonton for GOME2-A (middle left panel in Fig. 7), the intercept for the mismatched cases is significantly larger than the intercept for the matched cases; this behavior was also found for the 83% (GOME2A) and 91.2% (GOME2B) of the examined stations. For the matched cases the intercept can reach the value of 47 D.U. at maximum while, for the mismatched cases the intercept can reach the value of > 250 D.U. Considering all examined stations, the intercept for the matched cases was found to be 22.34 ± 3.98 D.U. for GOME2-A and 19.35 ± 4.32 D.U. for GOME2-B, while for the mismatched cases was found to be 31.93 ± 10.43 D.U. for GOME2-A and 31.68 ± 14.17 D.U. for GOME2-B.

For the OMI comparisons, due to the smaller spatial resolution and smaller radii of search, the mismatched cases were further classified in two subcases clarifying which measurement is outside the polar vortex, the satellite (hereafter, *sat out*) or the ground-based (hereafter, *gnd*

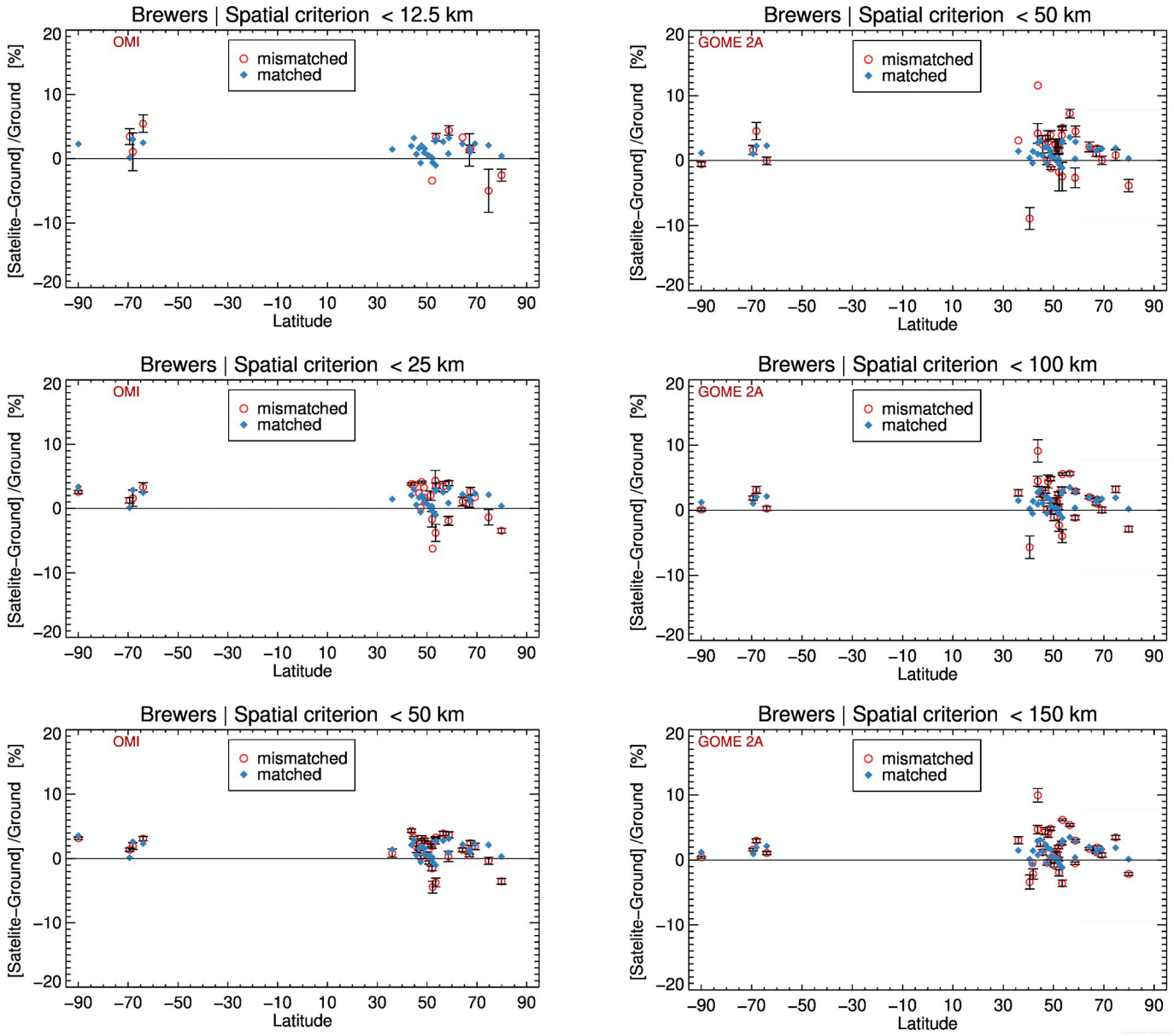

Fig. 4. Mean bias between OMI and Brewer (left column) and GOME2-A and Brewer (right column) TOC measurements as a function of latitude for the Brewer network. The collocated TOC measurements during winter-spring period are classified as mismatched (red circles) and matched (blue diamonds) with the spatial collocation criteria being within 12.5 km for OMI and 50 km for GOME2-A (top left and right), 25 km for OMI and 100 km for GOME2-A (middle left and right), 50 km for OMI and 150 km for GOME2-A (bottom left and right). (For interpretation of the references to colour in this figure legend, the reader is referred to the web version of this article.)

Table 3
Mean biases and number of collocations for the four selected stations for a 150 km spatial criterion for the GOME2-A for the mismatched and the matched cases.

Stations	lat	Mismatched		Matched	
		N	Mean bias (%) and 1σ/√N	N	Mean bias (%) and 1σ/√N
Edmonton	53.57	342	6.16 ± 0.15	74,851	3.02 ± 0.02
Resolute	74.72	232	3.46 ± 0.31	61,631	1.88 ± 0.02
Comodoro Rivadavia	−45.78	53	3.56 ± 0.47	58,497	3.50 ± 0.01
Marambio	−64.00	1135	1.09 ± 0.24	33,783	2.14 ± 0.03
Total average			2.22 ± 0.4		1.46 ± 0.17

Table 4
Mean biases and number of collocations for the four selected stations for a 150 km spatial criterion for the GOME2-B for the mismatched and the matched cases.

Stations	lat	Mismatched		Matched	
		N	Mean bias (%) and 1σ/√N	N	Mean bias (%) and 1σ/√N
Edmonton	53.57	138	6.57 ± 0.24	30,580	3.57 ± 0.03
Resolute	74.72	76	2.13 ± 0.42	33,755	3.03 ± 0.02
Comodoro Rivadavia	−45.78	48	4.04 ± 0.52	20,990	3.60 ± 0.02
Marambio	−64.00	441	0.54 ± 0.44	15,370	1.71 ± 0.04
Total average			1.84 ± 0.57		1.69 ± 0.22

Table 5
Mean biases and number of collocations for the four selected stations for a 50 km spatial criterion for the OMI for the mismatched and the matched cases.

Stations	lat	Mismatched		Matched	
		N	Mean bias (%) and 1σ/√N	N	Mean bias (%) and 1σ/√N
Goose	53.32	58	2.81 ± 0.51	18,765	2.58 ± 0.03
Vindeln	64.25	60	1.37 ± 0.28	13,964	2.20 ± 0.03
Macquarie Island	−54.48	27	4.64 ± 1.01	40,299	4.08 ± 0.02
Marambio	−64.00	401	3.11 ± 0.34	17,213	2.35 ± 0.04
Total average			1.93 ± 0.39		1.7 ± 0.19

out).The equivalent OMI scatter plots with the sat out mismatched subcases are shown in the left column of Fig. 8 while the scatter plots with the gnd out mismatched subcases are shown in the right column of Fig. 8. A similar overall pattern is seen as for the GOME2 comparisons but no further assessment can be made. Considering all OMI collocations, the correlation coefficient for the matched cases was found to be 0.95 ± 0.01, while for the sat out mismatched subcases it was found to be 0.9 ± 0.03 and for the gnd out mismatched subcases 0.94 ± 0.01.

4. Conclusions

In this work, we examined the space-borne total ozone columns depending on the location of the polar vortex when choosing collocation pairs to ground-based observations. OMI/Aura, GOME-2/Metop-A and Metop-B TOC measurements produced by the GODFIT (GOME-type Direct FITting) v4 algorithm were compared to TOC measurements from Brewer and Dobson spectrophotometers archived at the World Ozone and Ultraviolet Radiation Data Centre (WOUDC) repository. ERA-Interim reanalysis Potential Vorticity level estimates, extracted from the European Centre for Medium-Range Weather Forecasts (ECMWF), were used to

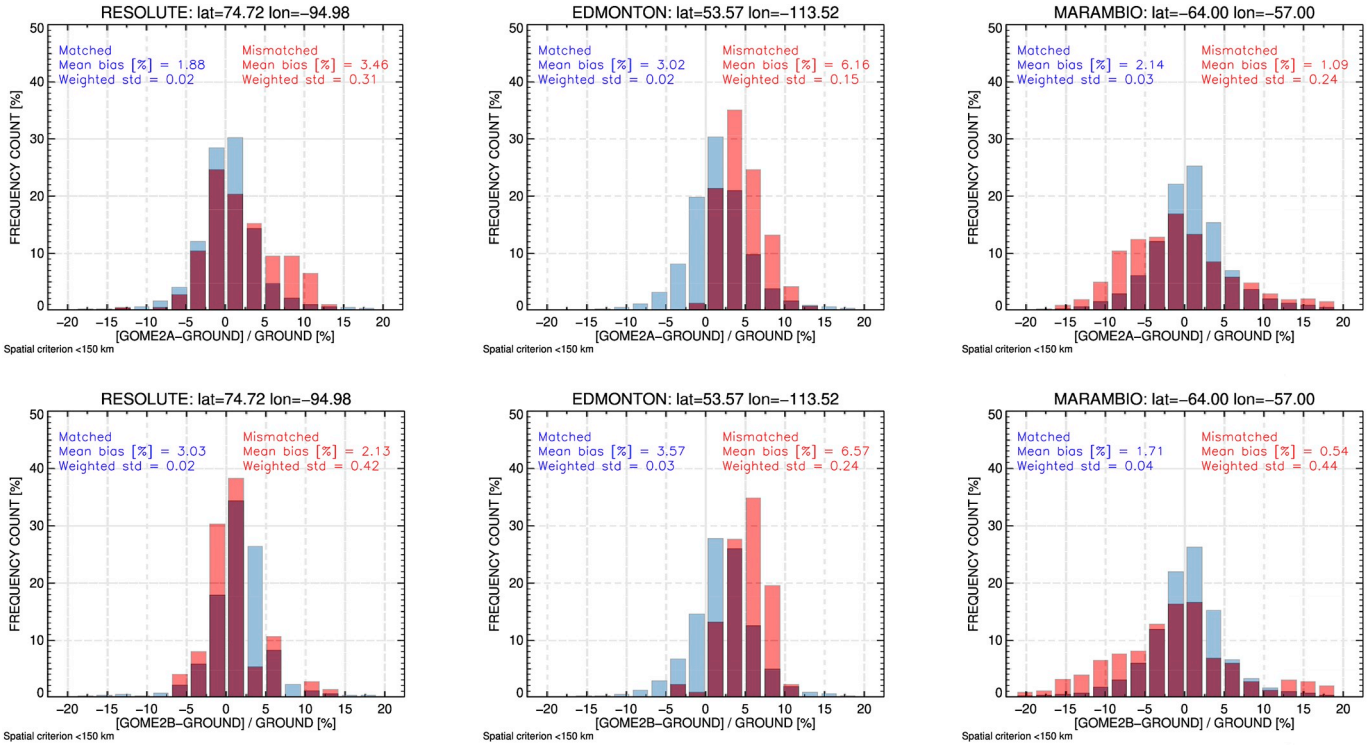

Fig. 5. Histograms of the bias for the matched (in blue) and mismatched (in red) cases in Resolute (left column), Edmonton (middle column) and Marambio (right column) for GOME2-A (top row), GOME2-B (bottom row) during the winter-spring period. (For interpretation of the references to colour in this figure legend, the reader is referred to the web version of this article.)

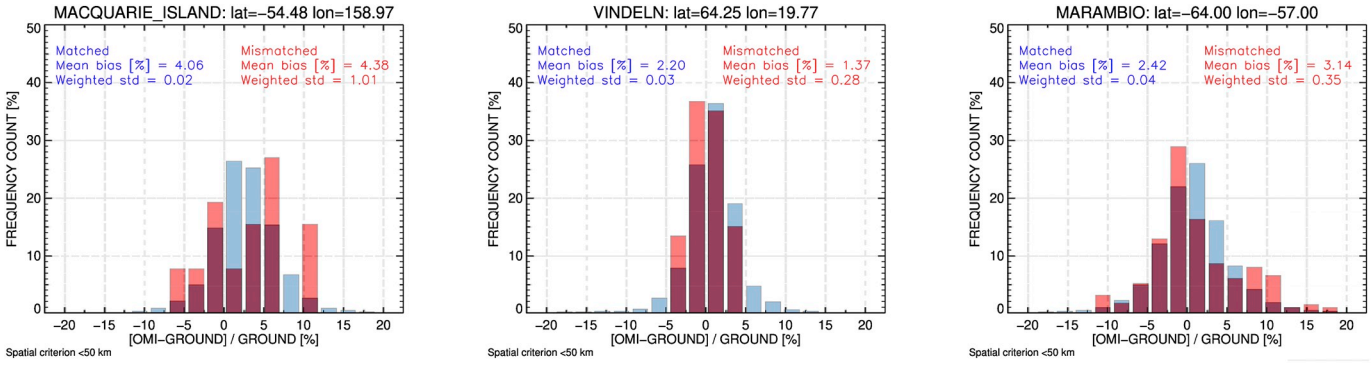

Fig. 6. Histograms of the bias for the matched (in blue) and mismatched (in red) cases in Macquarie Island (left), Vindeln (middle) and Marambio (right) for OMI during the winter-spring period. (For interpretation of the references to colour in this figure legend, the reader is referred to the web version of this article.)

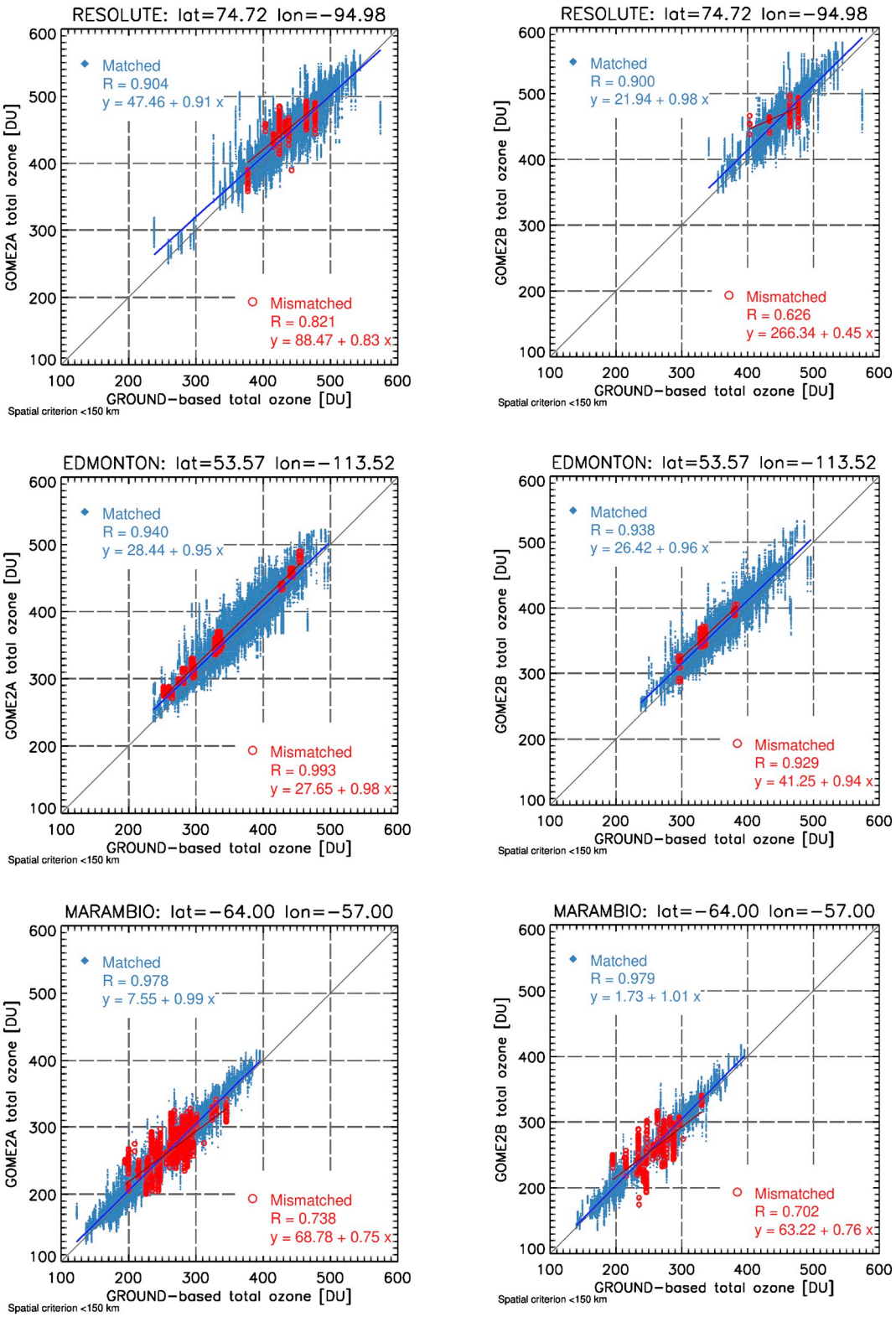

Fig. 7. Scatter plots between the ground based TOC measurements (x-axis) and the satellite TOC measurements (y-axis), for the matched (blue) and mismatched (red) cases in Resolute (top), Edmonton (middle) and Marambio (bottom).GOME2-A on the left column and GOME2-B on the right column. (For interpretation of the references to colour in this figure legend, the reader is referred to the web version of this article.)

locate the polar vortex edge and quantify whether either set of TOC observations were within or outside its perimeter.

For all collocations that belong to the winter-spring period of each hemisphere, for the middle and high latitude stations, the mean bias for the mismatched cases was found to be 2.22 ± 0.4%, 1.84 ± 0.57% and 1.93 ± 0.39%for GOME2-A, GOME2-B and OMI respectively, whereas for the matched cases 1.46 ± 0.17%, 1.69 ± 0.22%, 1.7 ± 0.19%. The global correlation coefficient was very similar for the two cases, at 0.95 ± 0.01 whereas the slope for the matched cases was found to be 0.97 ± 0.01, while the mismatched cases in total, the slope was found to

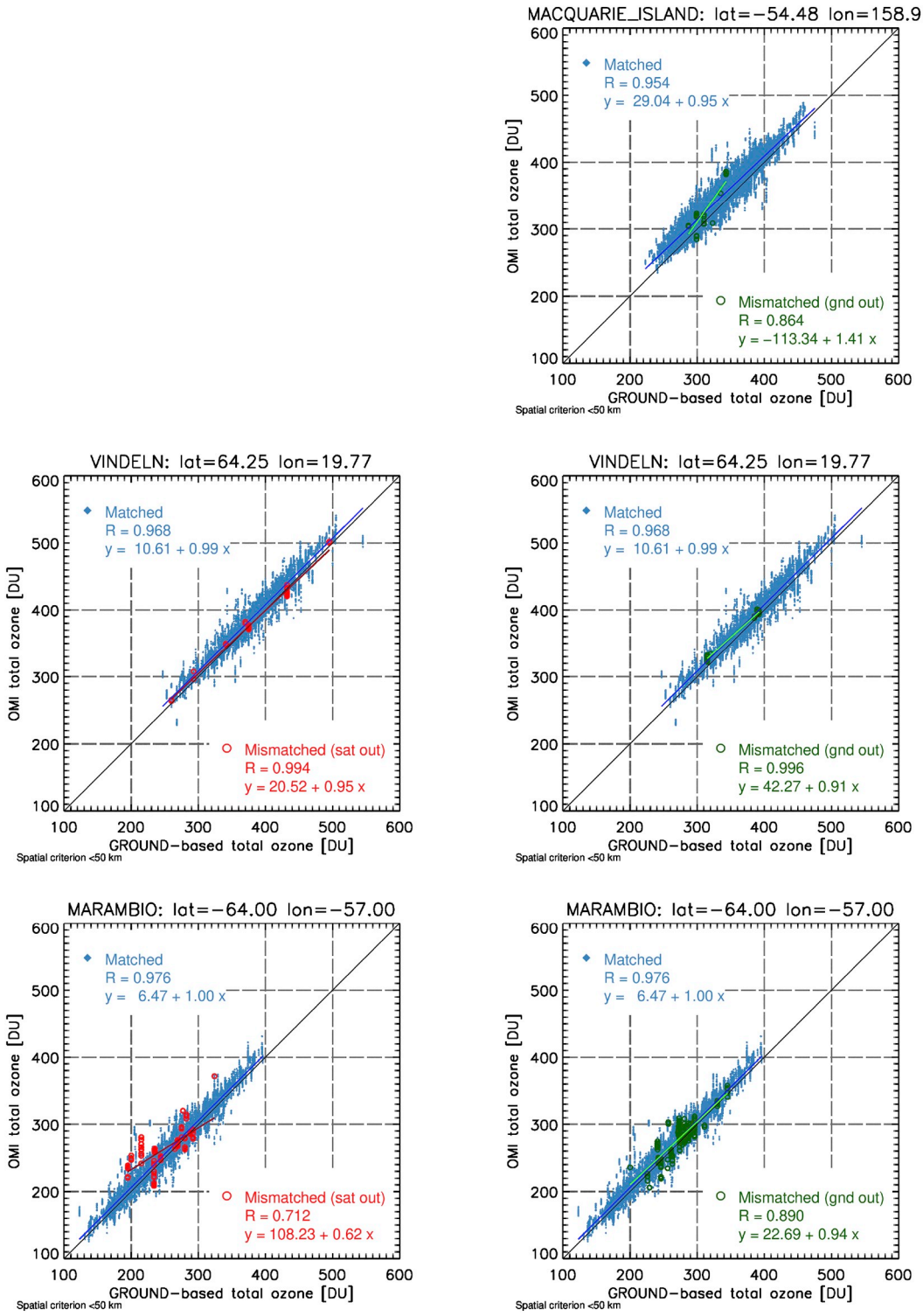

Fig. 8. Scatter plots with the ground based TOC measurements along the x axis and the OMI TOC measurements along the y axis on the left for the matched (blue) and sat out mismatched (red) cases and on the right for the matched (blue) and gnd out mismatched (green) cases, with the radius between satellite and ground < 50 km in Macquarie Island (top), Vindeln (middle) and Marambio (bottom). The upper left panel is empty since no sat out mismatched cases were found in Macquarie Island. (For interpretation of the references to colour in this figure legend, the reader is referred to the web version of this article.)

be 1.02 ± 0.03. Separating the mismatched cases into two sub-sets depending on whether the satellite or the ground observations was outside the vortex edges alters the slope to 0.92 ± 0.04 and 1.05 ± 0.03 respectively. The intercept for the matched cases was found to be 16.83 ± 3.38 D.U., while for the mismatched satellite subcases was found to be 29.07 ± 12.97 D.U. and for mismatched ground-based subcases was found to be −16.28 ± 10.94 D.U. Overall this study concludes that, when focusing on hemispherical or global findings, the merit of examining the location of the polar vortex vis-à-vis the spatial collocation criterion is rather low. However, it would be well worth the effort to add this extra check when comparing instantaneous ground-based observations on a per station basis.

Declaration of Competing Interest

None.

Acknowledgements

This research did not receive any specific grant from funding agencies in the public, commercial, or not-for-profit sectors. The authors are grateful to ESA's Ozone Climate Change Initiative project for providing the satellite borne data used in this publication. The ground-based data used in this publication were obtained from WMO's Global Atmosphere Watch (GAW) program and are publicly available via the World Ozone and UV Data Centre (WOUDC) (see https://woudc.org/). The potential vorticity data used in this work were provided by ERA-Interim reanalysis datasets from the European Centre for Medium-Range Weather Forecasts (ECMWF) (see https://www.ecmwf.int/). Finally, we would like to acknowledge and warmly thank all the investigators that provide data to these repositories on a timely basis, as well as the handlers of these databases for their upkeep and quality guaranteed efforts.

Appendix A

Table A.1
List of Brewer stations used in the comparisons.

ID	Name	Latitude	Longitude	Country
21	Edmonton	53.57	−113.52	Canada
24	Resolute	74.72	−94.98	Canada
35	Arosa	46.77	9.67	Switzerland
50	Potsdam	52.38	13.05	Germany
53	Uccle	50.8	4.35	Belgium
65	Toronto	43.78	−79.47	Canada
68	Belsk	51.83	20.78	Poland
76	Goose	53.32	−60.38	Canada
77	Churchill	58.75	−94.07	Canada
82	Lisbon	38.77	−9.13	Portugal
89	NyAlesund	78.93	11.88	Norway
96	HradecKralove	50.18	15.83	CzechRepublic
99	Hohenpeissenberg	47.80	11.02	Germany
100	Budapest	47.43	19.18	Hungary
111	Amundsen-Scott	−89.98	−24.80	Antarctica
123	Yakutsk	62.08	129.75	Russia
174	Lindenberg	52.22	14.12	Germany
213	ElArenosillo	37.10	−6.73	Spain
233	Marambio	−64.00	−57.00	Antarctica
241	Saskatoon	52.10	−105.28	Canada
261	Thessaloniki	40.52	22.97	Greece
262	Sodankyla	67.37	26.65	Finland
267	Sondrestrom	67.00	−50.98	Greenland
279	Norkoping	58.58	16.12	Sweden
282	Kislovodsk	43.73	42.66	Russia
284	Vindeln	64.25	19.77	Sweden
287	Funchal	32.65	−17.05	Portugal
290	Saturkeyna	48.78	−123.13	Canada
295	MtWaliguan	36.17	100.53	China
301	Ispra	45.80	8.63	Italy
305	RomeUniversity	41.90	12.52	Italy
308	Madrid	40.45	−3.55	Spain
309	Copenhagen	55.72	12.57	Denmark
315	Eureka	79.89	−85.93	Canada
316	Debilt	52.00	5.18	Netherlands
318	Valentia	51.93	−10.25	Irland
319	Montreal	45.47	−73.75	Canada
320	Winnipeg	49.91	−97.24	Canada
321	Halifax	44.90	−63.50	Canada
326	Longfenshan	44.75	127.60	China
331	Poprad-Ganovce	49.03	20.32	Slovakia
332	Pohang	36.03	129.38	Korea
338	Regina	50.21	−104.67	Canada
346	Murcia	38.00	−1.17	Spain
348	Ankara	39.95	32.88	Turkey
352	Manchester	53.45	−2.26	United Kingdom
353	Reading	51.42	−0.96	United Kingdom
376	MrsaMtrouh	31.33	27.22	Egypt
404	Jokioinen	60.80	23.50	Finland
405	LaCoruna	43.33	−8.50	Spain
411	Zaragoza	41.66	−0.94	Spain
447	Goddard	38.99	−76.83	U.S.A.
454	San Martin	−68.13	−67.10	Antarctica
476	Andoya	69.247	15.97	Norway
478	Zhongshan	−69.40	76.35	Antarctica
479	Aosta	45.71	7.33	Italy
481	Tomsk	56.48	84.97	Russia
512	UniversityOfToronto	43.63	−79.43	Canada
513	AnmyeonDo	36.54	126.33	Korea

Table A.2
List of Dobson stations used in the comparisons.

ID	Name	Latitude	Longitude	Country
7	Kagoshima	31.63	130.60	Japan
11	Quetta	30.18	66.95	Pakistan
12	Sapporo	43.05	141.33	Japan
13	Srinagar	34.08	74.83	India
14	Tateno	36.05	140.13	Japan
19	Bismarck	46.77	−100.75	U.S.A.
20	Caribou	46.87	−68.02	U.S.A.
29	MacquarieIsland	−54.48	158.97	Australia
35	Arosa	46.77	9.67	Switzerland
36	Camborne	50.22	−5.32	United Kingdom
40	HauteProvence	43.92	5.75	France
43	Lerwick	60.15	−1.15	United Kingdom
50	Potsdam	52.38	13.05	Germany
51	Reykjavik	64.13	−21.90	Iceland
53	Uccle	50.80	4.35	Belgium
57	HalleyBay	−75.52	−26.73	Antarctica
67	Boulder	40.02	−105.25	U.S.A.
68	Belsk	51.83	20.78	Poland
82	Lisbon	38.77	−9.13	Portugal
89	NyAlesund	78.93	11.88	Norway
91	Buenos-Aires	−34.58	−58.48	Argentina
92	Hobart	−42.88	147.33	Australia
96	HradecKralove	50.18	15.83	CzechRepublic
99	Hohenpeissenberg	47.80	11.02	Germany
100	Budapest	47.43	19.18	Hungary
101	Syowa	−69.00	39.58	Antarctica
105	Fairbanks	64.80	−147.89	U.S.A.
106	Nashville	36.25	−86.57	U.S.A.
107	WallopsIsland	37.87	−75.52	U.S.A.
111	Amundsen-Scott	−89.98	−24.80	Antarctica
116	Moscow	55.75	37.57	Russia
152	Cairo	30.08	31.28	Egypt
159	Perth	−31.95	115.85	Australia
165	Oslo	59.92	10.72	Norway
199	Barrow	71.32	−156.60	U.S.A.
201	Sestola	44.22	10.77	Italy
208	Shiangher	39.77	117.00	China
213	ElArenosillo	37.10	−6.73	Spain
226	Bucharest	44.48	26.13	Romania
232	Vernadsky-Faraday	−65.25	−64.27	Antarctica
252	Seoul	37.57	126.95	Korea
253	Melbourne	−37.48	144.58	Australia
256	Lauder	−45.03	169.68	NewZealand
268	ArrivalHeights	−77.83	166.40	Antarctica
284	Vindeln	64.25	19.77	Sweden
293	Athens	38.00	23.70	Greece
339	Ushuaia	−54.85	−68.31	Argentina
341	Hanford	36.32	−119.63	U.S.A.
342	ComodoroRivadavia	−45.78	−67.50	Argentina
343	Salto	−31.58	−57.95	Uruguay
419	Bordeaux	44.81	−0.56	France

References

Baldwin, M.P., Holton, J.R., 1988. Climatology of the Stratospheric Polar Vortex and Planetary Wave Breaking. J. Atmos. Sci. 45 (7), 1123–1142. https://doi.org/10.1175/1520-0469(1988)045<1123:COTSPV>2.0.CO;2.

Balis, D., Kroon, M., Koukouli, M.E., Brinksma, E.J., Labow, G., Veefkind, J.P., McPeters, R.D., 2007a. Validation of Ozone Monitoring Instrument total ozone column measurements using Brewer and Dobson spectrophotometer ground-based observations. J. Geophys. Res.-Atmos. 112 (24). https://doi.org/10.1029/2007JD008796.

Balis, D., Lambert, J.C., Van Roozendael, M., Spurr, R., Loyola, D., Livschitz, Y., ... Zehner, C., 2007b. Ten years of GOME/ERS2 total ozone data - The new GOME data processor (GDP) version 4: 2. Ground-based validation and comparisons with TOMS V7/V8. J. Geophys. Res. Atmos. *112* (7). https://doi.org/10.1029/2005JD006376.

Berrisford, P., Dee, D.P., Poli, P., Brugge, R., Fielding, M., Fuentes, M., ... Simmons, A, 2011. The ERA-Interim archive Version 2.0. 1. pp. 23.

Bhartia, P.K., McPeters, R.D., Flynn, L.E., Taylor, S., Kramarova, N.A., Frith, S., ... DeLand, M., 2013. Solar Backscatter UV (SBUV) total ozone and profile algorithm. Atmos. Measure. Tech. 6 (10), 2533–2548. https://doi.org/10.5194/amt-6-2533-2013.

Bojkov, R.D., Balis, D.S., Zerefos, C.S., 1998. Characteristics of the ozone decline in the northern polar and middle latitudes during the winter-spring. Meteorog. Atmos. Phys. 69 (1), 119–135. https://doi.org/10.1007/BF01025187.

Cede, A., Herman, J., Richter, A., Krotkov, N., Burrows, J., 2006. Measurements of nitrogen dioxide total column amounts using a Brewer double spectrophotometer in direct Sun mode. J. Geophys. Res.-Atmos. https://doi.org/10.1029/2005JD006585.

Diémoz, H., Siani, A.M., Redondas, A., Savastiouk, V., Mcelroy, C.T., Navarro-Comas, M., Hase, F., 2014. Improved retrieval of nitrogen dioxide (NO2) column densities by means of MKIV Brewer spectrophotometers. Atmos. Measure. Tech. https://doi.org/10.5194/amt-7-4009-2014.

Flynn, L.E., McNamara, D., Beck, C.T., Petropavlovskikh, I., Beach, E., Pachepsky, Y., ... Taylor, S., 2009. Measurements and products from the Solar Backscatter Ultraviolet (SBUV/2) and OOzone Mapping and Profiler Suite (OMPS) instruments. International Journal of Remote Sensing 30 (15–16), 4259–4272. https://doi.org/10.1080/01431160902825040.

Garane, K., Lerot, C., Coldewey-Egbers, M., Verhoelst, T., Koukouli, M.E., Zyrichidou, I., ... Zehner, C., 2018. Quality assessment of the OOzone_cci CClimate Research Data Package (release 2017) – Part 1: Ground-based validation of total ozone column data

products. Atmos. Meas. Tech. 11 (3), 1385–1402. https://doi.org/10.5194/amt-11-1385-2018.

Hansen, G., Dahlback, A., Tønnessen, F., Svenøe, T., 1999. Validation of GOME total ozone by means of the Norwegian ozone monitoring network. Ann. Geophys. 17 (3), 430–436. https://doi.org/10.1007/s00585-999-0430-9.

Hassinen, S., Balis, D., Bauer, H., Begoin, M., Delcloo, A., Eleftheratos, K., ... Zyrichidou, I., 2016. Overview of the O3M SAF GOME-2 operational atmospheric composition and UV radiation data products and data availability. Atmos. Meas. Tech. 9 (2), 383–407. https://doi.org/10.5194/amt-9-383-2016.

Hewitt, N.J., Jackson, A.V., 2009. Atmospheric Sci Ence for Environmental Scientists. Wiley-Blackwell, Chichester.

Hood, L., Rossi, S., Beulen, M., 1999. Trends in lower stratospheric zonal winds, Rossby wave breaking behavior, and column ozone at northern midlatitudes. J. Geophys. Res.-Atmos. 104 (D20), 24321–24339. https://doi.org/10.1029/1999JD900401.

Kerr, J.B., McElroy, C.T., Olafson, R.A., 1981. Measurements of ozone with the Brewer ozone spectrophotometer. In: Quadrennial International Ozone Symposium, Boulder, CO, pp. 74–79.

Koukouli, M.E., Lerot, C., Granville, J., Goutail, F., Lambert, J.-C., Pommereau, J.-P., ... Zehner, C., 2015. Evaluating a new homogeneous total ozone climate data record from GOME/ERS-2, SCIAMACHY/Envisat, and GOME-2/MetOp-A. J. Geophys. Res.-Atmos. 120 (23), 12,212–296,312. https://doi.org/10.1002/2015JD023699.

Koukouli, M.E., Zara, M., Lerot, C., Fragkos, K., Balis, D., van Roozendael, M., ... van der A, R.J., 2016. The impact of the ozone effective temperature on satellite validation using the Dobson spectrophotometer network. Atmos. Meas. Tech. 9 (5), 2055–2065. https://doi.org/10.5194/amt-9-2055-2016.

Kramarova, N.A., Frith, S.M., Bhartia, P.K., McPeters, R.D., Taylor, S.L., Fisher, B.L., ... DeLand, M.T., 2013. Validation of ozone monthly zonal mean profiles obtained from the version 8.6 Solar Backscatter Ultraviolet algorithm. Atmospheric Chemistry and Physics 13 (14), 6887–6905. https://doi.org/10.5194/acp-13-6887-2013.

Labow, G.J., McPeters, R.D., Bhartia, P.K., Kramarova, N., 2013. A comparison of 40 years of SBUV measurements of column ozone with data from the Dobson/Brewer network. J. Geophys. Res.-Atmos. 118 (13), 7370–7378. https://doi.org/10.1002/jgrd.50503.

Lerot, C., van Roozendael, M., Lambert, J.-C., Granville, J., van Gent, J., Loyola, D., Spurr, R., 2010. The GODFIT algorithm: a direct fitting approach to improve the accuracy of total ozone measurements from GOME. Int. J. Remote Sens. 31 (2), 543–550. https://doi.org/10.1080/01431160902893576.

Lerot, C., Van Roozendael, M., Spurr, R., Loyola, D., Coldewey-Egbers, M., Kochenova, S., ... Zehner, C., 2014. Homogenized total ozone data records from the European sensors GOME/ERS-2, SCIAMACHY/Envisat, and GOME-2/MetOp-A. J. Geophys. Res.-Atmos. 119 (3), 1639–1662. https://doi.org/10.1002/2013JD020831.

Levelt, P.F., Joiner, J., Tamminen, J., Veefkind, J.P., Bhartia, P.K., Stein Zweers, D.C., ... Wargan, K., 2018. The Ozone Monitoring Instrument: overview of 14 years in space. Atmos. Chem. Phys. 18 (8), 5699–5745. https://doi.org/10.5194/acp-18-5699-2018.

Loyola, D.G., Koukouli, M.E., Valks, P., Balis, D.S., Hao, N., Van Roozendael, M., ... Lambert, J.-C., 2011. The GOME-2 total column ozone product: retrieval algorithm and ground-based validation. J. Geophys. Res.-Atmos. 116 (D7). https://doi.org/10.1029/2010JD014675.

Munro, R., Lang, R., Klaes, D., Poli, G., Retscher, C., Lindstrot, R., ... Eisinger, M., 2016. The GOME-2 instrument on the Metop series of satellites: instrument design, calibration, and level 1 data processing – an overview. Atmos. Meas. Tech. 9 (3), 1279–1301. https://doi.org/10.5194/amt-9-1279-2016.

Nash, E.R., Newman, P.A., Rosenfield, J.E., Schoeberl, M.R., 1996. An objective determination of the polar vortex using Ertel's potential vorticity. J. Geophys. Res.-Atmos. 101 (D5), 9471–9478. https://doi.org/10.1029/96JD00066.

Parrondo, M.C., Gil, M., Yela, M., Johnson, B.J., Ochoa, H.A., 2014. Antarctic ozone variability inside the polar vortex estimated from balloon measurements. Atmos. Chem. Phys. https://doi.org/10.5194/acp-14-217-2014.

Pommereau, J.P., Goutail, F., 1988. O_3 and NO_2 ground-based measurements by visible spectrometry during Arctic winter and spring 1988. Geophys. Res. Lett. https://doi.org/10.1029/GL015i008p00891.

Redondas, A., Carreño, V., León-Luis, S.F., Hernández-Cruz, B., López-Solano, J., Rodriguez-Franco, J.J., ... Karppinen, T., 2018. EUBREWNET RBCC-E Huelva 2015 OOzone Brewer Intercomparison. Atmospheric Chemistry and Physics 18 (13), 9441–9455. https://doi.org/10.5194/acp-18-9441-2018.

Schoeberl, M.R., Hartmann, D.L., 1991. The dynamics of the stratospheric polar vortex and its relation to springtime ozone depletions. Science 251 (4989), 46–52. Retrieved from. http://www.jstor.org/stable/2875036.

Staehelin, J., Kerr, J., Evans, R., Vanicek, K., 2003. *Comparison of Total Ozone Measurements of Dobson and Brewer Spectrophotometers and Recommended Transfer Functions* (World Meteorological Organization. Gobal Atmosphere Watch) (Vol. 149). World Meteorological Organization.

Van Roozendael, M., Spurr, R., Loyola, D., Lerot, C., Balis, D., Lambert, J.-C., ... Zehner, C., 2012. Sixteen years of GOME/ERS-2 total ozone data: The new direct-fitting GOME Data Processor (GDP) version 5—Algorithm description. J. Geophys. Res.-Atmos. 117 (D3). https://doi.org/10.1029/2011JD016471.

Wallace, J.M., Hobbs, P.V., 2006. Atmospheric Science: An Introductory. Second Edition. Academic Press, Survey. https://doi.org/10.1016/C2009-0-00034-8.